Performance Analysis of Node-Assisted WiFi Backscatter Communication: A Stochastic Geometry Approach

Yulei Wang, Qinglin Zhao, *Senior Member, IEEE*, Shumin Yao, MengChu Zhou, *Fellow, IEEE*, Li Feng, and Peiyun Zhang, *Senior Member, IEEE*

***Abstract*—Node-assisted WiFi backscatter communication (NWB) is a promising technology that can extend the communication range of WiFi backscatters effectively and improve the backscatter throughput greatly. An NWB network consists of one access point (AP) and WiFi nodes, where the coverage area of a WiFi node contains many backscatter tags. In NWB, when detecting a transmitting WiFi excitation signal, tags concurrently contend to send their data to their respective WiFi nodes by backscattering the excitation signal, while these nodes later contend to relay their received tags' data to AP. In this paper, we develop a stochastic geometry-based model to analyze WiFi and backscatter throughputs. The challenges are three-folds: 1) how to model the randomness and dependency of WiFi and backscatter contentions, 2) how to model the location randomness of WiFi nodes and backscatter tags which are of repulsive or clustering characteristics, and 3) how to model the number of concurrent tag transmissions. With our model, we may select appropriate parameter settings (e.g., the density of WiFi nodes and backscatter tags) to improve the system performance. Extensive simulations are conducted to verify that our theoretical model is very accurate. The obtained outcomes can be used to provide proper parameter settings for achieving high NWB network performance.**

***Index Terms*—WiFi backscatter communication, stochastic geometry, Matérn hard-core point process, Matérn cluster process, performance analysis**

I. INTRODUCTION

TO date, WiFi networks have been extensively deployed in indoor and outdoor environments, offering widespread connectivity and strongly supporting the Internet-of-Things applications. WiFi backscatter communication [1], [2] exploits these ubiquitous WiFi signals as excitation signals to convey data and hence have broad application prospects in many fields [3]–[5]. Most existing studies of WiFi backscatter focus on one-hop communications between one WiFi device and backscatter tags (called tags for short) [1], [2], [6]. However, tags typically have very short transmission ranges (e.g., 1m to 54m [1], [7]) and low throughput, which greatly limits their practical deployments. Nevertheless, WiFi nodes possess much longer transmission ranges, which can be up to 1000m [8], [9], than backscatter tags. Recognizing this potential, Wang *et al.* [10] have recently proposed a node-assisted WiFi backscatter communication (NWB) scheme to extend tags' transmission range and improve the backscatter throughput.

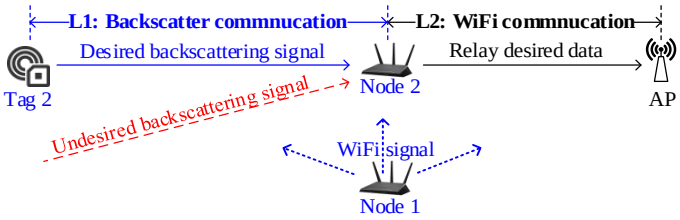

Fig. 1. An example of node-assisted WiFi backscatter.

An NWB network, as shown in Fig. 1, consists of one access point (AP) and multiple WiFi nodes (called nodes for short), where the coverage area of each node encompasses many tags. In NWB, tags' data transmission passes through two-level communications: tag-to-node backscatter-level and node-to-AP WiFi-level communications. Consider the scenario that tag 2 intends to send its data to AP via its node (i.e., node 2). In backscatter communications, assume that node 1 is transmitting WiFi signals to AP. Regarding these WiFi signals as excitation signals, tag 2 first wins the channel and then transmits its data to node 2 by backscattering these excitation signals. In WiFi communications, node 2 also first wins the channel and then relays tag 2's data to AP, where node 2's transmissions, just like node 1's transmissions, can be regarded as excitation signals by other nodes' tags. Essentially, while one node is relaying its received tag data to a remote AP, the ongoing WiFi signal triggers multiple tags to transmit their data to their respective nodes concurrently. As a result, NWB can extend tags' transmission range and improve the backscatter throughput.

A. Motivation

NWB is a long-range and high-throughput technology. In this paper, we aim to theoretically analyze the WiFi and backscatter throughputs of an NWB network and provide theoretically guided parameter settings for maximizing the system

- Y. Wang, Q. Zhao (corresponding author) and L. Feng are with the School of Computer Science and Engineering, Macau University of Science and Technology, Avenida Wei Long, Taipa, Macau, China (e-mail: wylpaper@126.com, qlzhao@must.edu.mo and lfeng@must.edu.mo).
- S. Yao is with the School of Computer Science and Engineering, Macau University of Science and Technology, Avenida Wei Long, Taipa, Macau, China, and also with the Department of Broadband Communication, Peng Cheng Laboratory, Shenzhen 518066, China (e-mail: zhysm@outlook.com).
- M. Zhou is with the Department of Electrical and Computer Engineering, New Jersey Institute of Technology, Newark, NJ 07102 USA (e-mail: zhou@njit.edu).
- P. Zhang is with the Engineering Research Center of Digital Forensics of Ministry of Education, and the School of Computer Science, Nanjing University of Information Science & Technology, Nanjing 210044, China (email: zpy@nuist.edu.cn; 20211220029@nuist.edu.cn).

performance. However, we face the following challenges. First, in NWB, data transmissions involve two-level contentions. It is challenging to model the dependency of the two-level contentions and characterize the impact of the contention randomness on the throughput. Second, the tags and nodes are randomly deployed in practical environments, where the deployment of nodes are of repulsive characteristics and that of tags are of clustering characteristics. It is challenging to model the location randomness of tags and nodes. Third, NWB enables multiple tags to transmit their data to their respective nodes concurrently. These concurrent transmissions may seriously interfere with the successful reception of tag data at nodes. It is challenging to model the number of interference links since not all tags transmit data concurrently. These challenges motivate this study.

B. Our Contributions

An NWB network consists of one AP and many randomly deployed tags and nodes. It adopts two-level communications (i.e., backscatter and WiFi-level communications) to extend tags' transmission range and improve the backscatter throughput. This study theoretically analyzes WiFi and backscatter throughputs of an NWB network. It intends to make the following novel contributions.

- It proposes a stochastic geometry (SG) approach to solve the aforementioned three modeling challenges. In NWB, backscatter communication depends on WiFi communications. Hence, it defines the same unit time for calculating WiFi and backscatter throughputs, thereby solving Challenge 1. Then it employs the Matérn hard-core point process and Matérn cluster process to capture nodes' repulsive characteristics and tags' clustering characteristics, respectively, hence solving Challenge 2. Next, it approximates the number of interference links by estimating the number of concurrent tag transmissions, solving Challenge 3.
- It expresses WiFi and backscatter throughputs in terms of the network parameters, design parameters, and the density of tags and WiFi nodes. With our model, we are able to select appropriate parameter settings (e.g., the density of tags and WiFi nodes) to improve the system performance.
- It performs extensive simulations to verify that our theoretical model is very accurate.

The rest paper is organized as follows. Section II presents the related work. Section III outlines the network topology and Medium Access Control (MAC) layer protocol of an NWB network. Section IV specifies the system model. Sections V and VI give the theoretical analysis of WiFi and backscatter throughputs, respectively. Section VII verifies the accuracy of our theoretical models via extensive simulations. Finally, Section VIII concludes the paper.

II. Related Work

Backscatter networks, in which tags exploit their surrounding excitation signals (e.g., television, cellular and WiFi signals) to convey data, have drawn great attention recently. This section presents existing work in terms of SG-based backscatter performance analysis and WiFi backscatter performance analysis.

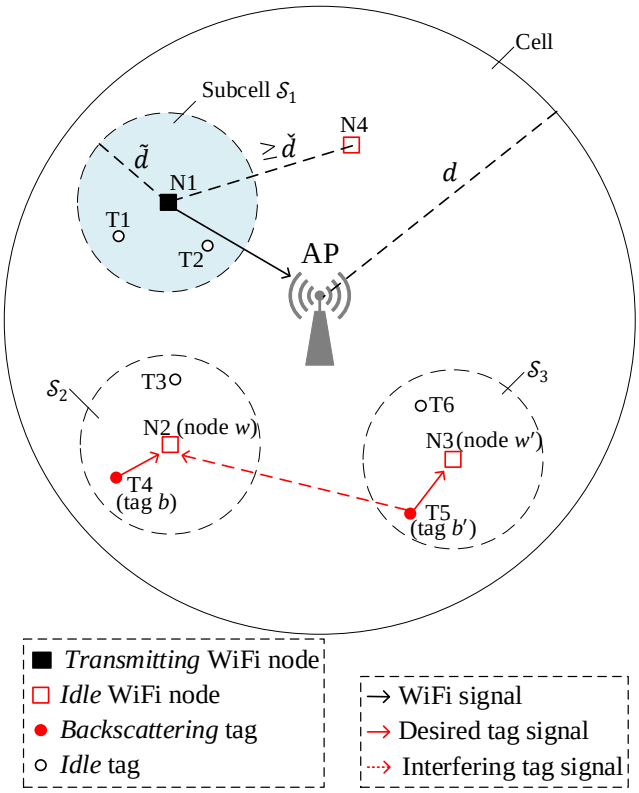

Fig. 2. A cell in an NWB network.

A. SG-based Backscatter Performance Analysis

Stochastic geometry, which is about the study of random spatial patterns, is widely used for modeling the impact of location randomness of devices on the performance of cellular networks [11], [12], ad hoc networks [13], WiFi networks [14], [15], and backscatter networks. For example, Wang *et al*. [16] and Han *et al*. [17] model multi-cluster backscatter networks, where the cluster centers (i.e., dedicated excitation signal emitters) and the tags within clusters are randomly distributed; they adopt SG to capture the location randomness of emitters, tags, and the inter-cluster and intra-cluster interferences. Different from our focused NWB, their concerned networks neither involve the contention process nor the MAC protocol of tags and hence their performance frameworks are not applicable in NWB.

B. WiFi Backscatter Performance Analysis

WiFi backscatter communication is a special case of backscatter communications. It can exploit ubiquitous WiFi signals to convey data and hence has broad application prospects in many fields. Existing studies mainly investigate the performances of one-hop and node-assisted WiFi backscatter networks.

Performance analysis of one-hop WiFi backscatter networks. Proof-of-concept one-hop single-link WiFi backscatter communications have been proposed in [1], [2], [18] and their performance evaluations are conducted via testbed to demonstrate the feasibility of WiFi backscatter communications. To improve the transmission efficiency, one-hop multi-link schemes have been proposed and analyzed recently. For example, Ma *et al*. [6] design and analyze a scheme that enables tags to contend

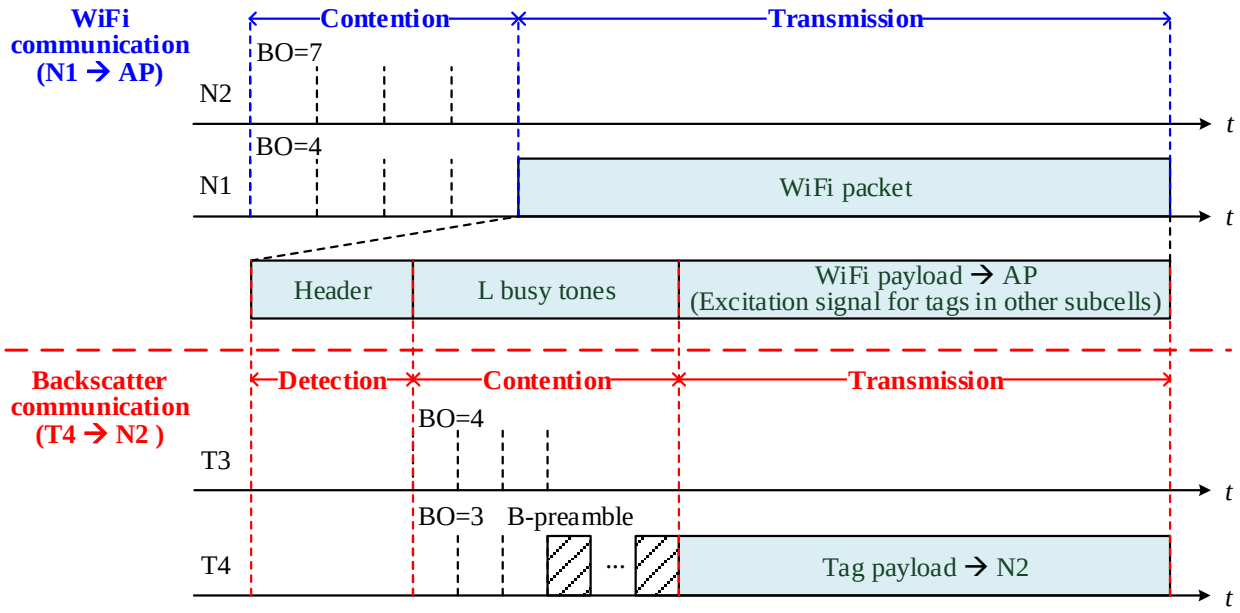

Fig. 3. An example of node-assisted tag transmissions in an NWB network.

to transmit their data to a single AP. Cao *et al.* [19] let an AP contend with WiFi nodes for providing WiFi backscatter communications and adopt an enhanced Markov chain to analyze the impact of the contention randomness on system throughput. However, their models do not consider the impact of the location distribution of tags on system throughputs. Our short paper [20] adopts an SG-based approach to investigate the impact of the location randomness of tags on the successful transmission probability of tags for a one-hop WiFi backscatter network. However, it does not capture the inherent dependency of tag and node contentions in node-assisted WiFi backscatter communications.

Performance analysis of node-assisted WiFi backscatter networks. One-hop WiFi backscatter networks generally have very short transmission ranges and low throughput. To address the two problems, Wang *et al.* [10] propose a node-assisted WiFi backscatter communication (NWB) scheme to significantly extend tags' transmission ranges and improve backscatter throughput. However, their performance analysis assumes ideal channel conditions, does not consider the location randomness of tag and nodes, and ignores the interferences due to concurrent tag-to-node transmissions. This paper proposes an SG-based approach that comprehensively and systematically investigates WiFi and backscatter throughputs. Our approach considers non-ideal channel conditions, the dependency of WiFi and backscatter contentions, the location randomness of tags and WiFi nodes, and the feature of concurrent tag transmissions. Hence, this paper significantly extends the work in [10] [20].

III. Node-Assisted WiFi Backscatter Communication

This section describes the network topology of a node-assisted WiFi backscatter (NWB) network and outlines its MAC layer protocol [10].

A. Network Topology

A typical NWB network, as shown in Fig. 2, consists of one access point (AP), randomly distributed WiFi nodes (called nodes for short) and backscatter tags (called tags for short). The coverage of the AP is a circular *cell* and it serves all nodes in the cell. The coverage of a node is a circular *subcell* and it serves all tags in its subcell. For example, the AP serves nodes N1, N2, and N3, while N2 serves T3 and T4.

B. MAC Layer Protocol

In an NWB network, the AP, nodes, and tags are half-duplex (i.e., each device either transmits or receives at the same time). Its MAC layer protocol consists of WiFi and backscatter-level protocols. The latter is designed based on the former, since the backscatter tags exploit the node-to-AP WiFi signals as excitation signals to transmit tag-to-node data. With the help of Fig. 3, we explain the two protocols.

1) WiFi-level Protocol

In WiFi communications, nodes first contend for the channel and then the winner transmits its data. In contention, nodes adopt a carrier-sense multiple access with collision avoidance mechanism and a binary exponential backoff algorithm to alleviate the contention collision. At the beginning of contention, each node chooses a backoff count (BO) uniformly distributed in $[0, \check{C} - 1]$, where $\check{C}$ is the minimum contention window size. After sensing the channel idle for a distributed interframe space (DIFS) time, it decreases its counter by one for each idle basic slot (i.e., a fixed minimum time unit) and suspends its counter for each busy basic slot. If its counter reaches zero, it transmits a packet to the AP and then waits for receiving an acknowledge (ACK) after a short interframe space (SIFS) time. If it cannot receive an ACK within a certain time (i.e., AckTimeout time), it infers that it experiences a collision. In case that a collision occurs, it doubles its contention window and enters a new backoff stage to retransmit the packet. When the backoff stage

limit is reached, it either transmits the packet successfully or drops the packet. In the example, N1's and N2's BOs are 4 and 7, respectively and N1 wins the contention and then transmits since its BO is the minimum one.

To assist tag-to-node communications, the WiFi-level protocol makes some modifications on the structure of a conventional WiFi packet. As shown in Fig. 3, a WiFi-level packet comprises three parts:

- Header. This part comprises a PHY preamble, a PHY header and an MAC header. It is the same as a conventional WiFi packet header except adding some additional fields such as signature (i.e., a special sequence). Each node has a unique signature and will add it to the packet header when transmitting a packet to the AP.
- L identical busy tones. This is a newly added part. Each busy stone is a dedicated sequence, which indicates tags to perform contention. A busy tone duration denotes the minimum time unit in the tag contention process. L denotes the contention window size of tags (i.e., the maximum number of time units in contention).
- WiFi payload. This part is the same as the conventional WiFi payload. The payload-transmission signal can be exploited as excitation signal of tags.

2) Backscatter-level Protocol

One backscatter communication process, as shown in Fig. 2 and Fig. 3, consists of three stages: detection, contention, and transmission. They correspond to the transmission stages of a WiFi packet's three parts: header, L identical busy tones, and WiFi payload, respectively.

In detection, each tag correlates its buffered node signatures with the received signal to detect if its node or other nodes are transmitting a WiFi packet. If the transmitting node is its node, it first calculates the transmission duration of the whole WiFi packet according to the duration field of the packet, and then remains idle until the next packet transmission. Otherwise, it harvests sufficient energy in the detection stage and then enters the contention and transmission stages. For example, in Fig. 2, T1 and T2 find that their node N1 is transmitting and hence keep idle in N1's transmission process. In contrast, T3 and T4 find that their node N2 does not transmit and hence harvest energy only in the detection stage.

In contention, each tag exploits the busy tones to perform contention and the winner transmits a predefined backscatter preamble (called B-preamble for short), which is unique for each subcell. At the beginning of contention, each tag chooses a BO uniformly distributed in $[0, L-1]$ and then starts counting down. For each time unit in contention, each tag performs two types of correlations: busy-tone and B-preamble correlations. If it detects a busy tone only, it decreases its counter by one, whereas only if it detects a B-preamble, it stops contention and remains idle until the end of the backscatter communication. When its counter reaches zero, it keeps broadcasting B-preamble until the end of the contention stage. For example, T3's and T4's initial BOs are 4 and 3, respectively. Hence T4 will win the contention and broadcast the B-preamble.

In transmission, the winning tag transmits its data to its node. For example, T4 transmits its data to N2. A node may receive three types of signals as shown in Fig. 1: (i) the WiFi signal, (ii) the desired tag signal, and (iii) the interfering tag signals. By exploiting the successive interference cancellation technology [21], [22], the node can first recognize and remove the WiFi signal, and then decode the desired signal from the remaining superposed signals [10].

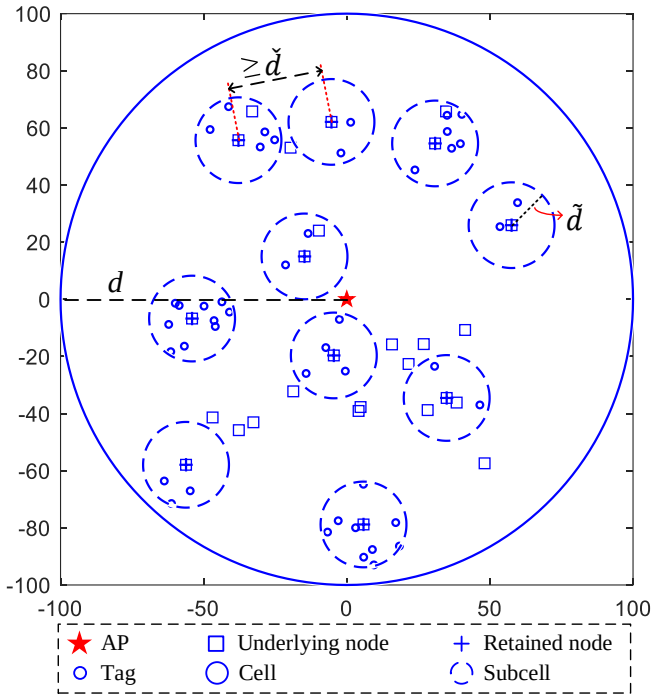

Fig. 4. A realization of spatial distributions of AP, underlying nodes following an HPPP, retained nodes following an MHCPP and tags following an MCP, where d = 100 m, $\tilde{d}$ = 15 m, $\check{d}$ = 30 m, λ_w^0 = 0.001 nodes/m^2, and Λ_b = 5 tags.

IV. System Model

In this section, we specify the system model of an NWB network, in terms of the spatial distributions of nodes and tags, the energy harvesting of tags, the interference and channel model, traffic model, and system throughput. For ease of reference, we summarize the used notations in Table I along with their corresponding descriptions.

A. Spatial Distribution

As shown in Fig. 2, we focus on a single-cell NWB network, where all nodes can hear each other. We use $A \subset \mathbb{R}^2$ with radius d to denote a circular *cell*. The cell consists of one AP, multiple nodes and numerous tags.

1) Matérn Hard-Core Point Process of Nodes

We employ Matérn hard-core point process of type II (called MHCPP for short) $\Phi_w \subset \mathbb{R}^2$ to model the spatial location distribution of nodes, which effectively captures the repulsive characteristics among nodes in a practical network. Specifically, an MHCPP Φ_w of nodes [23] is generated from a dependent thinning of homogeneous Poisson point process (HPPP) $\Phi_w^0 = \{\mathbf{x_i}, , i \in \mathbb{N}^+\} \subset \mathbb{R}^2$ of nodes with density λ_w^0, i.e., λ_w^0 nodes in a unit area. First, each node $\mathbf{x_i} \in \Phi_w^0$ is marked independently with a random label M_i where M_i is uniformly distributed in the interval $[0, 1]$. Then, $\mathbf{x_i} \in \Phi_w^0$ is retained in Φ_w if $\mathcal{D}(\mathbf{x_i}, \check{d})$ does not contain any point of Φ_w^0 with label smaller than M_i. The retained nodes form an MHCPP Φ_w, i.e.,

TABLE I
NOTIONS AND THEIR DESCRIPTIONS

Notation	Description
WiFi nodes	
Φ_w^0/λ_w^0	The underlying HPPP Φ_w^0 of nodes with density λ_w^0
$\Phi_w/\Phi_w^a/\lambda_w$	MHCPP Φ_w/approximated PPP Φ_w^a of nodes with density λ_w
Φ_w'/λ_w'	The set of non-transmitting nodes except w with density λ_w'
$\tilde{d}/\lvert\tilde{A}\rvert$	The radius/area of subcell $\tilde{A}$
$\check{d}$	The minimum distance between any two nodes
$M/\hat{m}$	The number of nodes in one cell with maximum value $\hat{m}$
$\mathbb{P}(m)$	The probability that there are m nodes in one cell
$\mathbb{P}_w^m$	The successful probability of one node-to-AP transmission
Ω	The generic slot duration representing the elapsed time of one backoff decrement in WiFi contention
ω	The duration of a basic slot for nodes
T_m^s	The time duration for a successful WiFi transmission
T_m^c	The time duration for an unsuccessful WiFi transmission
τ	The attempt rate of each node
γ	The collision probability experienced by each node
$\check{C}$	The minimum contention window size
K	The maximum backoff stage for nodes
$\mathbb{P}_w(Idle)$	The probability that the channel is idle for nodes
$\mathbb{P}_w(Succ)$	The probability of a successful WiFi transmission
$\mathbb{P}_w(Coll)$	The probability of a WiFi collision
$P_{b,w}$	The received desired signal power at node w from tag b
I	The received interfering signal power from tags
θ	The predefined SINR threshold
$R_{b,w}$	The distance between tag b and node w
$R_{b',w}$	The distance between interfering tag b' and node w
$f(\mathbf{y}\|\mathbf{x})$	The conditional PDF of $\mathbf{y}$ given an $\mathbf{x}$
$\tilde{f}_{R_{b,w}}(r_{b,w})$	The PDF of $R_{b,w}$
$\Gamma_w^m(\cdot)$	The WiFi throughput when there are m nodes in one cell
ξ	The number of successfully transmitted bits by nodes in one cell, during a unit time
Γ_w	The average WiFi throughput
Backscatter tags	
Φ_b/Λ_b	The MCP Φ_b of tags with mean Λ_b tags in one subcell
$\Phi_b'/\bar{\Psi}$	The set of interfering tags with mean $\bar{\Psi}$ tags in one subcell
P_0	The reflection power of each tag
H	The channel power gain of small-scale fading
α	The path-loss exponent
σ^2	Additive white Gaussian noise with variance σ^2
$N/\hat{n}$	The number of tags in a subcell with maximum value $\hat{n}$
$\mathbb{P}(n)$	The probability that there are n tags in a subcell
$\Psi/\bar{\Psi}$	Number/Mean # of tags that transmit concurrently in a subcell
L	The number of busy tones for tags
$\mathbb{P}_b^s$	The probability of a successful backscatter transmission
η	The number of successfully transmitted bits by tags within all subcells, during a unit time
Γ_b	The average backscatter throughput
AP	
$d/\lvert A\rvert$	The radius/area of cell A
System	
Γ_s	The average system throughput

$$\Phi_w \triangleq \left\{\mathbf{x_i} \in \Phi_w^0 : M_i < M_j, \forall\, \mathbf{x_j} \in \Phi_w^0 \cap \mathcal{D}\left(\mathbf{x_i}, \check{d}\right) \backslash \mathbf{x_i}\right\}$$

where $\mathcal{D}\left(\mathbf{x_i}, \check{d}\right)$ represents a disk centered at node $\mathbf{x_i} \in \Phi_w^0$ with radius $\check{d}$, and $\check{d}$ represents the minimum distance between any two nodes. Let p_w denote the probability that a random node $\mathbf{x_i} \in \Phi_w^0$ can be retained in Φ_w. According to [24], p_w is expressed as

$$p_w = \begin{cases} \dfrac{1 - \exp\left(-\lambda_w^0 \pi \check{d}^2\right)}{\lambda_w^0 \pi \check{d}^2} & \check{d} > 0 \\ 1 & \check{d} = 0 \end{cases}, \tag{1}$$

and the corresponding density λ_w of Φ_w can be obtained by weighting λ_w^0 with p_w, i.e.,

$$\lambda_w = p_w \lambda_w^0 \tag{2}$$

As studied in [23], [25], [26], [27], MHCPP Φ_w can be further approximated as HPPP Φ_w^a with same density λ_w, i.e.,

$$\Phi_w^a \approx \Phi_w \tag{3}$$

and the accuracy of such approximation is validated in [28]. Hence, the nodes within cell A are assumed to approximately follow uniform distribution in location and Poisson distribution with mean $\lambda_w|A|$, where $|A| = \pi d^2$ denotes the area of one cell. We use $\tilde{A} \subset \mathbb{R}^2$ with radius $\tilde{d}$ to denote a circular *subcell*, which is formed by one node.

2) Matérn Cluster Process of Tags

We employ the Matérn cluster process (MCP) $\Phi_b \subset \mathbb{R}^2$ to model the spatial location distribution of tags, which effectively captures the clustering characteristics of tags in a practical network [16]. According to [13], we can generate:

$$\Phi_b \triangleq \bigcup_{\mathbf{x_i} \in \Phi_w^a} \Phi_i + \mathbf{x_i} \tag{4}$$

where Φ_w^a is an HPPP defined in (3), and the offspring tags $\mathbf{y_i} \in \Phi_i$ are uniformly scattered in the subcell $\mathcal{D}\left(\mathbf{x_i}, \tilde{d}\right)$ centered at a parent node $\mathbf{x_i} \in \Phi_w^a$ with radius $\tilde{d}$, and follow Poisson distribution with mean Λ_b [29]. Let $\mathbf{x}$ and $\mathbf{y}$ respectively denote the Cartesian coordinates of a parent node and its one offspring tag, where the distribution of offspring tags around the parent node in each subcell are independent and identically distributed (i.i.d.) with the same spatial probability density function (PDF). Let R_y represent the Euclidean distance between an offspring tag $\mathbf{y}$ and its parent node $\mathbf{x}$, i.e., $R_y = \|\mathbf{x} - \mathbf{y}\|$. Given an $\mathbf{x}$, the conditional PDF $f(\mathbf{y}|\mathbf{x})$ is expressed as

$$f(\mathbf{y}|\mathbf{x}) = \frac{1}{\pi \tilde{d}^2}, 0 \le R_y \le \tilde{d} \tag{5}$$

Let $\tilde{f}_{R_y}(r_y)$ denote the PDF of R_y. Then $\tilde{f}_{R_y}(r_y)$ can be expressed as

$$\tilde{f}_{R_y}(r_y) = \frac{2r_y}{\tilde{d}^2}, 0 \le r_y \le \tilde{d} \tag{6}$$

To facilitate the analysis, we give the probability generating functional (PGFL) of an MCP Φ_b in advance. For any function $v(\mathbf{y})$: $\mathbb{R}^2 \to [0,1]$ and $\int_{\mathbb{R}^2}\left(1 - v(\mathbf{y})\right) d\mathbf{y} < \infty$, the PGFL of an MCP Φ_b is given as [13], [30], [31], [32]:

$$G(v) = \mathbb{E}\left[\prod_{\mathbf{y} \in \Phi_b} v(\mathbf{y})\right] = \exp\left(-\lambda_w \int_{\mathbb{R}^2}\left[1 - \exp\left(-\Lambda_b \int_{\mathbb{R}^2}\left(1 - v(\mathbf{y}' + \mathbf{x})\right) f(\mathbf{y}'|\mathbf{x}) d\mathbf{y}\right)\right] d\mathbf{x}\right) \tag{7}$$

where $\mathbf{x}, \mathbf{y} \in \Phi_b$ are coordinates with respect to the origin $\boldsymbol{o}(0,0)$, $\mathbf{y}'$ is the coordinate with respect to $\mathbf{x}$ where $\mathbf{y}'$ and $\mathbf{y}$ are different representations of the same point under different reference points, and $f(\mathbf{y}'|\mathbf{x})$ is given as that in (5).

In Fig. 4, we depict a realization of spatial distributions of AP, underlying nodes following an HPPP, retained nodes following an MHCPP, and tags following an MCP.

B. Energy Harvesting of Tags

As shown in Fig. 3, a whole transmission process of a tag consists of three stages: detection, contention, and transmission. In this paper, to concentrate on our main contributions, we

assume that each tag can harvest sufficient energy in the detection stage for contention and data transmission. On one hand, this assumption is feasible. For example, as shown in Fig. 3, we may add a special field (e.g., energy tones) after the WiFi header, so as to increase the detection time which spans the transmission time of the WiFi header and the special field. As long as the detection time is sufficiently long, tags can harvest sufficient energy in the detection stage. On the other hand, like [16], [17], we may extend our framework to model the number of tags that can harvest sufficient energy. For example, let Λ_b' denote the mean number of tags in each subcell which can harvest sufficient energy in the detection stage. Let p_b be the probability that one tag can harvest sufficient energy, which is related to the distance between energy emitters and the tag as well as the energy harvesting efficiency of the tag. Since Λ_b is the total mean number of tags in each subcell, we have $\Lambda_b' = p_b\Lambda_b$.

C. Interference and Channel Model

In an NWB network as shown in Fig. 2, when a node N1 in subcell $\mathcal{S}_1$ is transmitting a packet to the AP, tag b in subcell $\mathcal{S}_2$ may transmit its data to its node w by backscattering this N1-to-AP signal. In general, when one node in $\mathcal{S}_1$ transmits a WiFi signal to the AP, tags in all subcells except $\mathcal{S}_1$ may transmit their data to their respective nodes by backscattering this WiFi signal. Before proceeding with the interference model, we make two assumptions:

1. Tag transmissions will not interfere with the node-to-AP transmission. The reason is as follows. The received tag signal power at the AP is far less than the received node power [33], [34], and hence the AP may adopt successive interference cancellation [21], [22] to extract WiFi signals successfully. Because of Assumption 1, in this paper, we do not analyze the impact of tags' transmissions on WiFi throughput.

2. The node-to-AP WiFi transmission will not interfere with tag-to-node transmissions (say, the N1-to-AP transmission will not interfere with the b-to-w transmission), since node w may exploit successive interference cancellation to remove WiFi signal and further decode the desired b-to-w signal [10], [21], [22], as explained in the last paragraph of Section III.B.2).

In general, these WiFi and tag signals do not mutually interfere with each other.

However, when tag b in $\mathcal{S}_2$ transmits its data to its node w, other tag transmissions in other subcells such as $\mathcal{S}_3$ may interfere with this b-to-w transmission. Let $\Phi_b' \subset \Phi_b$ be a set of interfering tags that interfere with a desired tag transmission (e.g., the b-to-w tag transmission). Φ_b' does not contain the tags in the subcell where the node is transmitting a WiFi signal to the AP; for example, Φ_b' excludes the tags in $\mathcal{S}_1$. The interference level from Φ_b' depends on the location and number of nodes and tags is modeled in Section VI. To capture this impact of these interferences on the tag transmissions, we consider that each tag signal undergoes both large and small-scale channel fading [35]. We assume that the former follows a path loss model $r^{-\alpha}$, where r is the Euclidean distance between a tag and its node, and $\alpha, 2 < \alpha < 6$, is the path-loss exponent [16], [36]. We assume that each channel power gain H in the latter is independent and identically distributed with an exponential distribution with mean $1/\mu$, i.e., $H \sim \text{Exp}(\mu)$ [37], [38]. For example, consider the b-to-w transmission. Let P_0 denote the reflection power of each tag. Let $P_{b,w}$ denote the received signal power from tag b at the node w. Let $H_{b,w}$ and $R_{b,w}$ be the channel power gain and the distance between tag b and node w, respectively. According to the above channel model, we have:

$$P_{b,w} = P_0 H_{b,w} R_{b,w}^{-\alpha} \tag{8}$$

Further, let I denote the interference power that node w suffers, which is mainly from the interference of tags in Φ_b' due to Assumption 2. I can be expressed as

$$I = \sum_{b' \in \Phi_b'} P_0 H_{b',w} R_{b',w}^{-\alpha} \tag{9}$$

where $H_{b',w}$ and $R_{b',w}$ are the channel power gain and the distance between tag b' and node w, respectively.

In addition, we assume an additive white Gaussian noise channel with zero mean and variance σ^2.

D. Traffic Model

Like [39], [40], to investigate the system capacity, we assume saturated traffic, namely, each WiFi node and each tag always have data to transmit.

E. System Throughput

For an NWB network, under the above assumptions, we adopt a stochastic geometry approach to investigate its system throughput. We define the average system throughput Γ_s as the sum of the average WiFi throughput Γ_w and the average backscatter throughput Γ_b. That is,

$$\Gamma_s = \Gamma_w + \Gamma_b \tag{10}$$

In the following two sections, we calculate Γ_w and Γ_b sequentially. Particularly, our theoretical model captures the impact of the contention, location, and number of WiFi nodes on the backscatter throughput.

V. WiFi Throughput

This section analyzes the average WiFi throughput Γ_w.

Let ξ be the WiFi throughput representing the number of successfully transmitted bits by WiFi nodes in one cell, during a unit time. Let $\mathbb{E}[\xi]$ be the mean of ξ. Then we have

$$\Gamma_w \triangleq \mathbb{E}[\xi] \tag{11}$$

According to the WiFi-level protocol, nodes first contend for the channel successfully and then transmit packets. The number of nodes affects the probability of winning the contention and hence the WiFi throughput ξ. Let M denote the number of nodes in one cell. Let $\mathbb{P}(m) \triangleq \Pr(M = m)$ be the probability mass function of M. Recall that the nodes follow HPPP Φ_w^a with density λ_w defined in (3) and the number of nodes in one cell follows a Poisson distribution with mean $\lambda_w|A|$. Hence, $\mathbb{P}(m)$ is given as:

$$\mathbb{P}(m) = \exp(-\lambda_w|A|)\frac{(\lambda_w|A|)^m}{m!} \tag{12}$$

Then, according to the law of total expectation, we have:

$$\mathbb{E}[\xi] = \sum_{m=1}^{\hat{m}} \mathbb{P}(m)\,\mathbb{E}[\xi|m] \tag{13}$$

where m takes a value from 1 to a maximum value $\hat{m}$.

Next, we calculate $\mathbb{E}[\xi|m]$ by following the method in [39], [41], [42]. Let Ω denote a generic slot duration representing the elapsed time of one backoff decrement in WiFi contention. Let $\mathbb{E}[\Omega|m]$ denote the mean of Ω when m nodes contend for the

channel and regard $\mathbb{E}[\Omega|m]$ as the unit time for calculating the average throughput $\mathbb{E}[\xi|m]$. Let $\mathbb{P}_w(Succ|m)$ denote the probability of a successful node-to-AP transmission when m nodes contend for the channel. Then, $\mathbb{E}[\xi|m]$ can be expressed as

$$\mathbb{E}[\xi|m] = \frac{\mathbb{P}_w(Succ|m) \cdot L_w}{\mathbb{E}[\Omega|m]} \tag{14}$$

where L_w is the average WiFi packet size (measured in bits).

We proceed to give the expressions of $\mathbb{P}_w(Succ|m)$ and $\mathbb{E}[\Omega|m]$, since they are also used in the calculation of backscatter throughput in Section VI. Let τ denote the rate that each node attempts to transmit a packet when m nodes contend for the channel. In the following, we calculate τ, $\mathbb{P}_w(Succ|m)$, and $\mathbb{E}[\Omega|m]$ sequentially.

A. Calculation of τ

For a single-cell WiFi network with m nodes, the attempt rate τ is governed by the following fixed-point equation [39], [40]:

$$\begin{cases} \tau = \dfrac{2}{1 + \check{C} + \gamma\check{C}\sum_{k=0}^{K-1}(2\gamma)^k} \\ \gamma = 1 - (1-\tau)^{m-1} \end{cases} \tag{15}$$

where γ denotes the collision probability that each node experiences in channel contention, $\check{C}$ and K are the minimum contention window and the maximum backoff stage, respectively.

B. Calculation of $\mathbb{P}_w(Succ|m)$

In WiFi, one node-to-AP transmission is successful when only one among m nodes attempts to transmit a packet. Hence, $\mathbb{P}_w(Succ|m)$ can be expressed as

$$\mathbb{P}_w(Succ|m) = m\tau(1-\tau)^{m-1}. \tag{16}$$

C. Calculation of $\mathbb{E}[\Omega|m]$

In WiFi, time is divided into a series of basic slots, where a basic slot is the predefined minimum time unit. Given m, the generic slot duration, $\Omega|m$, depends on whether one basic slot is idle, and whether one transmission is successful or unsuccessful. We have

$$\Omega|m = \begin{cases} \omega & \mathbb{P}_w(Idle|m) \\ T_m^s & \mathbb{P}_w(Succ|m) \\ T_m^c & \mathbb{P}_w(Coll|m) \end{cases} \tag{17}$$

where ω is the duration of a basic slot, $\mathbb{P}_w(Succ|m)$ is given in (16), and other variables are defined as follows.

- T_m^s is one successful WiFi transmission time, including packet transmission time T_{Packet}, SIFS time T_{SIFS}, ACK time T_{ACK}, and DIFS time T_{DIFS}. Hence, we have:
$$T_m^s = T_{Packet} + T_{SIFS} + T_{ACK} + T_{DIFS}. \tag{18}$$
- T_m^c is one unsuccessful WiFi transmission time, i.e.,
$$T_m^c = T_{Packet} + T_{ACKTimeout} + T_{DIFS} \tag{19}$$
where $T_{ACKTimeout}$ is one AckTimeout time and can be set to $T_{ACK} + T_{SIFS}$ [6].
- $\mathbb{P}_w(Idle|m)$ is the probability that a basic slot is idle, namely, the probability that none among m nodes attempt to transmit a packet in one basic slot. We have
$$\mathbb{P}_w(Idle|m) = (1-\tau)^m. \tag{20}$$
- $\mathbb{P}_w(Coll|m)$ is the probability that one node experiences a collision when m nodes contend for the channel and is given as:
$$\mathbb{P}_w(Coll|m) = 1 - \mathbb{P}_w(Idle|m) - \mathbb{P}_w(Succ|m) \tag{21}$$
From (17), we can easily express $\mathbb{E}[\Omega|m]$:
$$\mathbb{E}[\Omega|m] = \omega\mathbb{P}_w(Idle|m) + T_m^s\mathbb{P}_w(Succ|m) + T_m^c\mathbb{P}_w(Coll|m). \tag{22}$$

VI. BACKSCATTER THROUGHPUT

This section analyzes the average backscatter throughput Γ_b.

Let η be the backscatter throughput representing the number of successfully transmitted bits by backscatter tags within all subcells, during a unit time. Let $\mathbb{E}[\eta]$ be the mean of η. Then we have

$$\Gamma_b \triangleq \mathbb{E}[\eta] \tag{23}$$

According to this definition, the average backscatter throughput is related to the number of all subcells. Since one node forms one subcell, the number of all nodes in a cell, m, is the number of all subcells. According to the law of total expectation, we have:

$$\mathbb{E}[\eta] = \sum_{m=1}^{\hat{m}} \mathbb{P}(m)\,\mathbb{E}[\eta|m] \tag{24}$$

where $\mathbb{P}(m)$ is the probability that there are m nodes in one cell and is given in (12), and m takes a value from 1 to a maximum value $\hat{m}$. Below, we give the expression of $\mathbb{E}[\eta|m]$.

We first model the unit time in the definition of the backscatter throughput. Recall that tags' transmissions depend on one node-to-AP transmission. For example, as shown in Fig. 2, when node N1 wins the WiFi-level contention and starts transmitting its packet to the AP, upon sensing this N1-to-AP signal, tags in each subcells except $\mathcal{S}_1$ first contend for the channel and then the winning tag transmits its data to its node, e.g., tag b in $\mathcal{S}_2$ transmits one data to node w. When analyzing the WiFi throughput in Section V, we use $\mathbb{E}[\Omega|m]$, which is given in (22), to denote the unit time. During the duration $\mathbb{E}[\Omega|m]$, if there is a node transmitting its packet to the AP, the winning tags can transmit their data to their respective nodes. Hence, we also use $\mathbb{E}[\Omega|m]$ to denote the unit time to calculate $\mathbb{E}[\eta|m]$.

Then, we express $\mathbb{E}[\eta|m]$. Let us focus on subcell $\mathcal{S}_2$ in Fig. 2 to first analyze the backscatter throughput in one subcell. Let $\mathbb{P}_b^s$ be the successful probability that a tag in one cell transmits one data to its node (e.g., tag b in $\mathcal{S}_2$ transmits one data to node w). Then, the backscatter throughput in $\mathcal{S}_2$ can be expressed as $\frac{\mathbb{P}_b^s \cdot L_b}{\mathbb{E}[\Omega|m]}$, where L_b is the average backscatter data size (measured in bits). Now, we express the backscatter throughput of all subcells. Given m nodes in one cell, when one node in one cell transmits its packet to the AP, tags in $m-1$ subcells (except the subcell formed by the transmitting node) may transmit their data to their respective nodes in parallel. Hence, we have:

$$\mathbb{E}[\eta|m] = (m-1) \cdot \mathbb{P}_w(Succ|m) \cdot \frac{\mathbb{P}_b^s \cdot L_b}{\mathbb{E}[\Omega|m]} \tag{25}$$

where $\mathbb{P}_w(Succ|m)$ and $\mathbb{E}[\Omega|m]$ are given in (16) and (22), respectively. Below, we calculate $\mathbb{P}_b^s$, which is related to two types of randomness: (i) the contention randomness of tags in one subcell, and (ii) the location randomness of tags and nodes. Let us focus on $\mathcal{S}_2$ in Fig. 2 again. Let N denote the number of tags in $\mathcal{S}_2$. Let Ψ denote the number of tags that win and transmit in

$\mathcal{S}_2$ simultaneously. Let $\mathbb{P}(\Psi=1,N=n)$ denote the probability that n tags are in $\mathcal{S}_2$ but only one tag wins the channel. Let $\mathbb{P}(RX\_succ|\Psi=1)$ denote the probability that the transmission of the winning tag is successfully received by its node, on condition that only one tag wins the channel and transmits in $\mathcal{S}_2$. Consider that tag b in $\mathcal{S}_2$ transmits one data to node w. According to the backscatter-level protocol, one successful b-to-w transmission should satisfy two conditions: (C1) only tag b wins the contention and transmits and (C2) tag b 's transmission is successfully received by node w. Therefore, given $N=n$ tags in $\mathcal{S}_2$, one successful b-to-w transmission probability is $\mathbb{P}(\Psi=1,N=n)\cdot\mathbb{P}(RX\_succ|\Psi=1)$. Since N may take a value from 1 to the maximum value $\hat{n}$, we express $\mathbb{P}_b^s$ as:

$$\mathbb{P}_b^s=\sum_{n=1}^{\hat{n}}\mathbb{P}(\Psi=1,N=n)\cdot\mathbb{P}(RX\_succ|\Psi=1) \tag{26}$$

In (26), $\mathbb{P}(\Psi=1,N=n)$ is related to the contention randomness of tags in one subcell, while $\mathbb{P}(RX\_succ|\Psi=1)$ is related to the location randomness of tags and nodes. In the next two subsections, we calculate the two probabilities sequentially.

A. Probability That a Tag Wins & Transmits $\mathbb{P}(\Psi=1,N=n)$

For $1\le\psi\le n$, we give a general expression of $\mathbb{P}(\Psi=\psi,N=n)$, from which we may calculate $\mathbb{P}(\Psi=1,N=n)$. Let $\mathbb{P}(n)\triangleq\Pr(N=n)$ be the probability mass function of N. Let $\mathbb{P}(\Psi=\psi|n)$ be the probability that ψ tags win the contention and transmit when n tags contend for the channel in one subcell. The joint probability of Ψ and N is given as:

$$\mathbb{P}(\Psi=\psi,N=n)=\mathbb{P}(n)\mathbb{P}(\Psi=\psi|n) \tag{27}$$

1) Calculation of $\mathbb{P}(n)$

Recall that the tags follow MCP Φ_b and the number of tags in each subcell follows a Poisson distribution with mean Λ_b. Hence, $\mathbb{P}(n)$ is given as:

$$\mathbb{P}(n)=\exp(-\Lambda_b)\frac{(\Lambda_b)^n}{n!} \tag{28}$$

2) Calculation of $\mathbb{P}(\Psi=\psi|n)$

Depending on whether ψ is equal to n, we have

$$\mathbb{P}(\Psi=\psi|n)=\begin{cases}L\left(\frac{1}{L}\right)^{\psi} & \psi=n\\ \sum_{l=0}^{L-2}\binom{n}{\psi}\left(\frac{1}{L}\right)^{\psi}\left(\frac{L-1-l}{L}\right)^{n-\psi} & \psi<n\end{cases} \tag{29}$$

According to the backscatter-level protocol, during the contention, each tag in a subcell uniformly chooses one backoff counter from 0,1, …, $L-1$ for countdown, where L is the number of busy tones. The tag that chooses the minimum backoff counter is the winner. Let l, $l=0,1,\dots,L-1$, denote the minimum backoff counter in one contention process. With the help of Fig. 5, we calculate $\mathbb{P}(\Psi=\psi|n)$ in terms of $\psi=n$ and $\psi<n$.

When $\psi=n$, each tag chooses the same l with probability $1/L$ and hence all tags are all winners with probability $(1/L)^{\psi}$. Since l may take L values from 0 to $L-1$, we obtain the top expression in (29).

When $\psi<n$, ψ tags are winners and at least one tag is the loser. Each of ψ tags chooses the same l with probability $1/L$,

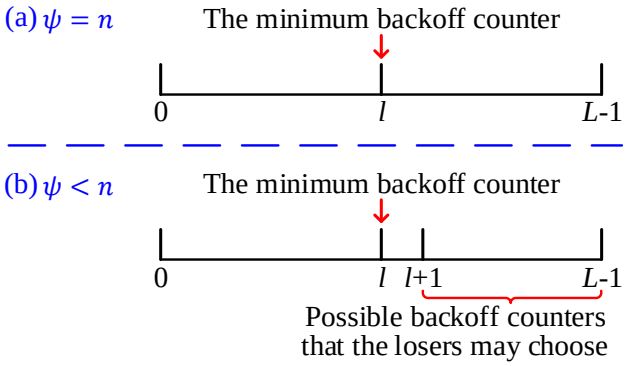

Fig. 5. Calculation of $\mathbb{P}(\Psi=\psi|n)$.

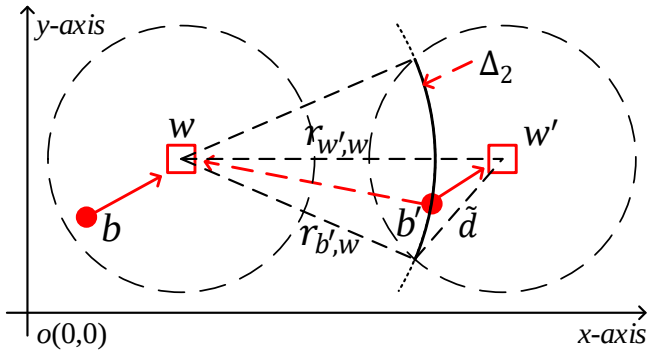

Fig. 6. Node w's received desired signal from tag b and interfering signal from tag b'.

while each of the remaining $n-\psi$ tags chooses one backoff count from $l+1$ to $L-1$ with probability $(L-1-l)/L$. Taking into account all possible values that l may take and the combination number of tags being winners $\binom{n}{\psi}$, we obtain the bottom expression in (29).

B. Probability That a Tag-to-node Transmission is Successfully Received $\mathbb{P}(RX\_succ|\Psi=1)$

In a tag-to-node transmission, as shown in Fig. 6, a node $w\in\Phi_w$ receives a desired signal from a tag $b\in\Phi_b$ in $\mathcal{S}_2$ and interfering signals from interfering tags $b'\in\Phi_b'\subset\Phi_b$ when b' is transmitting to its node $w'\in\Phi_{w'}\subset\Phi_w$, where $\Phi_{w'}$ represents the set of non-transmitting nodes except node w. In a point process, with probability one, no two or more points coincide in the same location (or coordinate) [43]. In this paper, when mentioning a node w, we mean that the node is located in the coordinate w that is also used to denote the node itself. In Fig. 6, the coordinates, w, w', b and b' are under the same reference point $o(0,0)$ in a two-dimensional plane.

Let $R_{b,w}$ denote the distance between tag b and node w. Let I denote the power of the interference that node w suffers, where I is given in (9). Let $SINR(R_{b,w},I)$ denote the signal-to-interference-plus-noise ratio (SINR) between node w 's received power of the desired signal from tag b, $P_{b,w}$, and its suffered interference power I plus noise power σ^2. We may express $SINR(R_{b,w},I)$ as:

$$SINR(R_{b,w},I)=\frac{P_{b,w}}{I+\sigma^2}=\frac{P_0H_{b,w}R_{b,w}^{-\alpha}}{I+\sigma^2} \tag{30}$$

where $P_{b,w}$ is given in (8) and is a function of tag b's reflection power P_0, the channel power gain $H_{b,w}$, and the distance $R_{b,w}$.

In our model, node w successfully receives a signal from tag b if its measured SINR exceeds a predefined threshold θ (i.e., $SINR(R_{b,w}, I) > \theta$). Thus, we have:

$$\begin{aligned}
&\mathbb{P}(RX_succ|\Psi = 1) \\
&= \mathbb{E}_{I,R_{b,w}}\left[\mathbb{P}\left(SINR(R_{b,w}, I) > \theta\right)\right] \\
&= \mathbb{E}_I\left[\mathbb{E}_{R_{b,w}}\left[\mathbb{P}\left(SINR(R_{b,w}, I) > \theta\right)\right]\right] \\
&= \mathbb{E}_I\left[\int_0^{\tilde{d}}\left[\mathbb{P}\left(SINR(r_{b,w}, I) > \theta\right)\right] \cdot \tilde{f}_{R_{b,w}}(r_{b,w})\, dr_{b,w}\right] \\
&= \int_0^{\tilde{d}} \mathbb{E}_I\left[\mathbb{P}\left(SINR(r_{b,w}, I) > \theta\right)\right] \cdot \tilde{f}_{R_{b,w}}(r_{b,w}) dr_{b,w}
\end{aligned} \tag{31}$$

where $\tilde{d}$ is the radius of a subcell, $\tilde{f}_{R_{b,w}}(r_{b,w})$ is the PDF of $R_{b,w}$. According to the definition of MCP, $\tilde{f}_{R_{b,w}}(r_{b,w})$ is expressed as that in (6).

We then express $\mathbb{E}_I\left[\mathbb{P}\left(SINR(r_{b,w}, I) > \theta\right)\right]$ in (31) as

$$\begin{aligned}
&\mathbb{E}_I\left[\mathbb{P}\left(SINR(r_{b,w}, I) > \theta\right)\right] = \mathbb{E}_I\left[\mathbb{P}\left(\frac{P_0 H_{b,w} r_{b,w}^{-\alpha}}{I + \sigma^2} > \theta\right)\right] \\
&= \mathbb{E}_I\left[\mathbb{P}\left(H_{b,w} > \frac{\theta r_{b,w}^{\alpha}(I + \sigma^2)}{P_0}\right)\right] \\
&\overset{(a)}{=} \mathbb{E}_I\left[\exp\left(-\frac{\mu\theta r_{b,w}^{\alpha}}{P_0}(I + \sigma^2)\right)\right] \\
&= \exp\left(-\frac{\mu\theta r_{b,w}^{\alpha}}{P_0}\sigma^2\right)\mathbb{E}_I\left[\exp\left(-\frac{\mu\theta r_{b,w}^{\alpha}}{P_0} I\right)\right] \\
&\overset{(b)}{=} \exp(-s\sigma^2) \cdot \mathcal{L}_I(s)
\end{aligned} \tag{32}$$

where (a) holds because $H_{b,w}$ follows an exponential distribution with mean $1/\mu$, i.e., $H_{b,w} \sim \mathrm{Exp}(\mu)$. Eq. (b) holds because the Laplace transform of the interference I, $\mathcal{L}_I(s) = \mathbb{E}[\exp(-sI)]$, where $s = \frac{\mu\theta r_{b,w}^{\alpha}}{P_0}$. Note that the interference I that node w suffers depends on the set of interfering tags Φ_b'. We next calculate $\mathcal{L}_I(s)$.

1) Calculation of $\mathcal{L}_I(s)$

Taking into account Φ_b', we can obtain:

$$\begin{aligned}
&\mathcal{L}_I(s) = \mathbb{E}_I[\exp(-sI)] \\
&= \mathbb{E}_{R_{b',w},H_{b',w}}\left[\exp\left(-s\sum_{b'\in\Phi_b'} P_0 H_{b',w} R_{b',w}^{-\alpha}\right)\right] \\
&\overset{(a)}{=} \mathbb{E}_{R_{b',w}}\left[\mathbb{E}_{H_{b',w}}\left[\exp\left(-s\sum_{b'\in\Phi_b'} P_0 H_{b',w} R_{b',w}^{-\alpha}\right)\right]\right] \\
&\overset{(b)}{=} \mathbb{E}_{R_{b',w}}\left[\prod_{b'\in\Phi_b'} \mathbb{E}_{H_{b',w}}\left(\exp\left(-sP_0 R_{b',w}^{-\alpha} H_{b',w}\right)\right)\right] \\
&\overset{(c)}{=} \mathbb{E}_{R_{b',w}}\left[\prod_{b'\in\Phi_b'} \int_0^{\infty} \exp\left[-g(b',w)h_{b',w}\right] f\left(h_{b',w}\right) dh_{b',w}\right] \\
&\overset{(d)}{=} \mathbb{E}_{R_{b',w}}\left[\prod_{b'\in\Phi_b'} \int_0^{\infty} \exp\left[-g(b',w)h_{b',w}\right] \mu\exp\left(-\mu h_{b',w}\right) dh_{b',w}\right] \\
&= \mathbb{E}_{R_{b',w}}\left[\prod_{b'\in\Phi_b'} \left(\frac{\mu}{\mu + g(b',w)}\right)\right]
\end{aligned} \tag{33}$$

In (33), Eq. (a) holds because $R_{b\prime,w}$ and $H_{b\prime,w}$ are mutually independent. Eq. (b) is due to the exponentiation identity. Eq. (c) follows from the definition of expectation of $R_{b',w}$, where $g(b',w) \triangleq sP_0 R_{b',w}^{-\alpha}$, and $R_{b',w} = \|b' - w\|$. Eq. (d) holds because $H_{b',w}$ is exponentially distributed with mean $1/\mu$, i.e., $f\left(h_{b',w}\right) = \mu\exp\left(-\mu h_{b',w}\right)$. Recall that (i) the interfering tags Φ_b' of node w do not include the tags in the subcell of the transmitting node (i.e., subcell $\mathcal{S}_1$) and in the subcell of node w (i.e., subcell $\mathcal{S}_2$); (ii) the location of interfering tags Φ_b' also depends on the location of non-transmitting nodes in the set of $\Phi_{w'}$. However, like [17], [31], we may regard Φ_b' as an MCP with mean $\bar{\Psi}$ tags in each subcell, i.e., average $\bar{\Psi}$ concurrently transmitting tags in each subcell. Let $v(b') \triangleq \frac{\mu}{\mu + g(b',w)}$. With the help of Figs. 2 and 6, according to the PGFL of MCP, the last equation of (33) becomes

$$\begin{aligned}
&\mathcal{L}_I(s) = \mathbb{E}\left[\prod_{b'\in\Phi_b'} v(b')\right] \\
&= \exp\left(-\lambda_w' \int_{\mathcal{A}}\left[1 - \exp\left(-\bar{\Psi}\int_{\mathcal{B}}\left(1 - v(b'' + w')\right) f(b''|w') db''\right)\right] dw'\right)
\end{aligned} \tag{34}$$

where w' is the node with interfering tag b'' located within its subcell, λ_w' is the density of $\Phi_{w'}$, and $\mathcal{A}$ is the area in which the node w' locate. Recall that $\mathcal{A}$ excludes the subcell of the transmitting node (i.e., subcell $\mathcal{S}_1$) and the subcell of node w (i.e., subcell $\mathcal{S}_2$) in one cell. For the ease of analysis, we approximate $\mathcal{A}$ by a circular disk $\mathcal{D}(w, d)$ centered at node w with radius d. $\mathcal{B}$ is the area in which the interfering tags b'' locate. We express $\mathcal{B}$ as a circular disk $\mathcal{D}\left(w', \tilde{d}\right)$ centered at node w' with radius $\tilde{d}$. It should be noted that b'' is the Cartesian coordinate with respect to w', which is a different coordinate representation of b' under different reference points. Hence, we can use $b'' + w'$ to express b'.

In (34), $v(b'' + w')$ can be further expressed as

$$v(b'' + w') = \frac{\mu}{\mu + sP_0\|b'' + w' - w\|^{-\alpha}} = \frac{\mu}{\mu + sP_0\|b' - w\|^{-\alpha}} \tag{35}$$

Set $\mu = 1$, i.e., $H \sim \mathrm{Exp}(1)$. Then we convert (34) from Cartesian coordinates to polar coordinates [16], [31], i.e.,

$$\mathcal{L}_I(s) = \exp\left(-2\pi\lambda_w' \int_{\check{d}}^{\tilde{d}} (1 - \Delta_1)\, R_{w',w} dR_{w',w}\right) \tag{36}$$

in which

$$\begin{aligned}
\Delta_1 &= \exp\left(-\bar{\Psi}\int_{r_{inf}}^{r_{sup}} \frac{\|b' - w\|^{-\alpha}}{(sP_0)^{-1} + \|b' - w\|^{-\alpha}} \tilde{f}_{R_{b',w}}(r_{b',w}|R_{w',w}) dr_{b',w}\right) \\
&= \exp\left(-\bar{\Psi}\int_{r_{inf}}^{r_{sup}} \frac{r_{b',w}^{-\alpha}}{\left(\theta r_{b,w}^{\alpha}\right)^{-1} + r_{b',w}^{-\alpha}} \tilde{f}_{R_{b',w}}(r_{b',w}|R_{w',w}) dr_{b',w}\right)
\end{aligned} \tag{37}$$

where $\tilde{f}_{R_{b',w}}\left(r_{b',w}|R_{w',w}\right)$ is the conditional PDF of the distance between interfering tags b' and receiver node w, and $r_{inf} = r_{w',w} - \tilde{d}$, $r_{sup} = r_{w',w} + \tilde{d}$. Then, we can express $\tilde{f}_{R_{b',w}}\left(r_{b',w}|R_{w',w}\right)$ as

$$\tilde{f}_{R_{b',w}}(r_{b',w}|R_{w',w}) = \begin{cases} \frac{\Delta_2}{\pi \check{d}^2} & r_{b',w} \in [r_{inf}, r_{sup}], \\ 0 & \text{otherwise} \end{cases} \quad (38)$$

where Δ_2 is the arc as shown in Fig. 6, and the distance between the interfering tags b' lying on Δ_2 and w is always same. In our work, we set $\check{d} \geq \tilde{d}$, i.e., $r_{inf} \geq 0$ to avoid the distance between any two nodes too close. Then we can express Δ_2 as

$$\Delta_2 = 2r_{b',w}\arccos\left(\frac{r_{w',w}^2 + r_{b',w}^2 - \check{d}^2}{2r_{w',w}r_{b',w}}\right) \quad (39)$$

Numerical evaluation on the integral form of (36) is time consuming and may not provide significant insights. To address this, we present an asymptotic analysis for $\mathcal{L}_I(s)$ below.

Asymptotic analysis: When $\check{d} \to 0$, $d \to \infty$, applying the channel model in Eq. (8) and Lemma 1 in [32], we can obtain a closed-form lower bound to approximate the value of $\mathcal{L}_I(s)$. Thus, we can express (36) as

$$\begin{aligned} \mathcal{L}_I(s) &\geq \exp\left(-\pi\lambda'_w(sP_0)^{\frac{2}{\alpha}}\frac{1}{\text{sinc}(2/\alpha)}\right) \\ &= \exp\left(-\pi\lambda'_w\bar{\Psi}r_{b,w}^2\theta^{\frac{2}{\alpha}}\frac{1}{\text{sinc}(2/\alpha)}\right) \end{aligned} \quad (40)$$

In (40), the lower bound of $\mathcal{L}_I(s)$ depends on λ'_w and $\bar{\Psi}$. Below, we calculate them, respectively.

2) Calculation of λ'_w

Here, we calculate the density λ'_w of nodes forming the subcells that contain interfering tags of Φ'_b. Note that $\mathbb{E}(\Phi'_w(A))$ is the average number of interfering subcells in A when node w is receiving a desired tag transmission. We have

$$\lambda'_w = \frac{\mathbb{E}(\Phi'_w(A))}{|A|} \quad (41)$$

As shown in Fig. 2, when N1 in $\mathcal{S}_1$ is transmitting a packet to the AP, tag b in $\mathcal{S}_2$ regards this transmitting signal as the excitation signal and contends for the channel. When tag b wins the channel and starts transmitting its data to node w, all other tags in $\mathcal{S}_2$ will not transmit. In addition, all tags in $\mathcal{S}_1$ will not transmit. Therefore, $\mathcal{S}_1$ and $\mathcal{S}_2$ are not interfering subcells. In one cell, all subcells except the two subcells are interfering subcells. Note that one node forms one subcell. We can express $\mathbb{E}(\Phi'_w(A))$ as

$$\mathbb{E}(\Phi'_w(A)) = \mathbb{E}(\Phi_w(A)) - 2 \quad (42)$$

where $\mathbb{E}(\Phi_w(A)) = \lambda_w|A|$ is the mean number of nodes in the cell.

3) Calculation of $\bar{\Psi}$

Let $\mathbb{E}(\Psi)$ be the mean of Ψ. Then we have

$$\bar{\Psi} \triangleq \mathbb{E}(\Psi) \quad (43)$$

Recall that the average number of interfering tags Ψ in each subcell is associated with the number of tags n in each subcell. Let $\mathbb{E}(\Psi|n)$ denote the average number of transmitting tags in one interfering subcell. Hence, we have

$$\mathbb{E}(\Psi) = \mathbb{E}(\mathbb{E}(\Psi|n)) = \sum_{n=1}^{\hat{n}} \mathbb{E}(\Psi|n) \cdot \mathbb{P}(n) \quad (44)$$

where $\mathbb{P}(n)$ is given in (28) and $\mathbb{E}(\Psi|n)$ is expressed as

TABLE II
DEFAULT PARAMETER VALUES

Parameters	Description	Value
R_{data}	Data Rate of MCS 8	7.8 Mbps
R_{basic}	Basic Rate	0.65 Mbps
T_{SIFS}	Duration of one SIFS interval	160 μs
T_{DIFS}	Duration of one DIFS interval	264 μs
ω	Duration of a basic slot	52 μs
L_w	WiFi packet size	1000 *bytes*
PHY Header	Duration of PHY header	160 μs
MAC Header	(40bytes+4bytes) @R_{data}	46 μs
Route Header	20bytes@R_{data}	21 μs
Header	PHY + MAC + Route Header	227 μs
T_w	1000bytes@R_{data}	1026 μs
L_b	Backscatter packet size	26 bits
T_{ACK}	(24bytes+14bytes) @R_{basic}	39 μs
$T_{ACKTimeout}$	ACKTimeout time	199 μs
$\check{C}$	Minimum contention window size	16
K	Maximum backoff stage	7
L	Number of busy tones	8
T_{tone}	Duration of each busy tone	16 μs
d	Radius of one cell	100 m
$\check{d}$	Radius of each subcell	5 m

$$\mathbb{E}(\Psi|n) = \sum_{\psi=1}^{n} \psi \cdot \mathbb{P}(\Psi = \psi|n) \quad (45)$$

where $\mathbb{P}(\Psi = \psi|n)$ is given in (29).

VII. MODEL VERIFICATION

We conduct extensive simulations to verify the accuracy of our theoretical model and compare our model with that in [10], which assumes ideal channel conditions and does not consider the location distribution characteristics of nodes and tags, and ignores the interferences.

Our simulator is developed based on MATLAB 2018a. This simulator integrates the MAC module of NWB from [10], the white Gaussian noise generator module, the spatial distribution module in Section III.A and the channel module in Section III.C. We set WiFi parameters according to [8] and NWB parameters according to [10]. The default parameter settings are shown in Table II. Each simulation value is obtained from a simulation run of 400 seconds; a longer simulation time just yields negligible fluctuations. In all figures, the labels 'ana' and 'sim' denote the theoretical and simulation results, respectively.

A. Verification of $\mathbb{P}(\Psi = \psi|n)$ and $\bar{\Psi}$

We respectively verify the accuracy of $\mathbb{P}(\Psi = \psi|n)$ and $\bar{\Psi}$ in (29) and (43) as the number of tags n and the mean number of tags Λ_b in a subcell varies under different setting of the number of busy tones L.

Fig. 7 shows the impacts of different L (i.e., $L = 4, 8, 12$) on $\mathbb{P}(\Psi = \psi|n)$ with $\psi = 1, 2$, as n varies from 1 to 50. From this figure, we can conclude:

- Given L, as n increases, $\mathbb{P}(\Psi = 1|n)$ decreases. It is because that more tags in a subcell lead to more serious contention. The probability of only one tag winning the contention gradually decreases. While as n increases, $\mathbb{P}(\Psi = 2|n)$ first increases for more contention, and then gradually decreases for more tags (i.e., $\Psi > 2$) concurrently wining the contention. Besides, the tendency of the curve of the

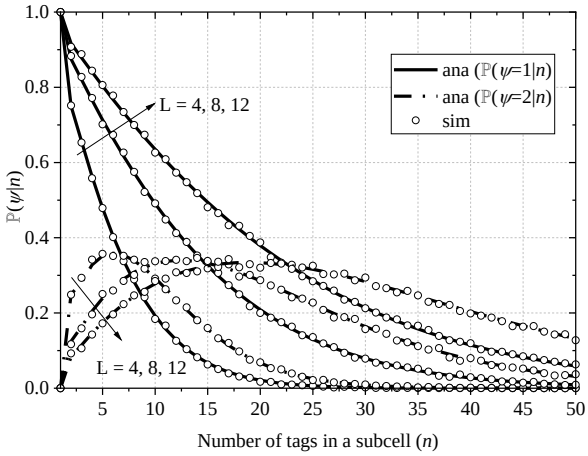

Fig. 7. $\mathbb{P}(\Psi = \psi|n)$ versus n under $L = 4, 8, 12$.

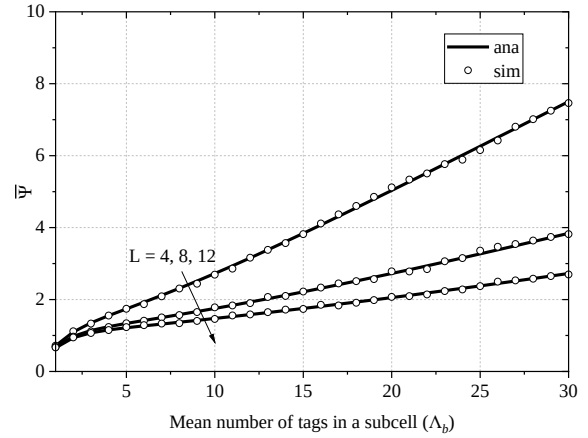

Fig. 8. $\bar{\Psi}$ versus Λ_b under $L = 4, 8, 12$.

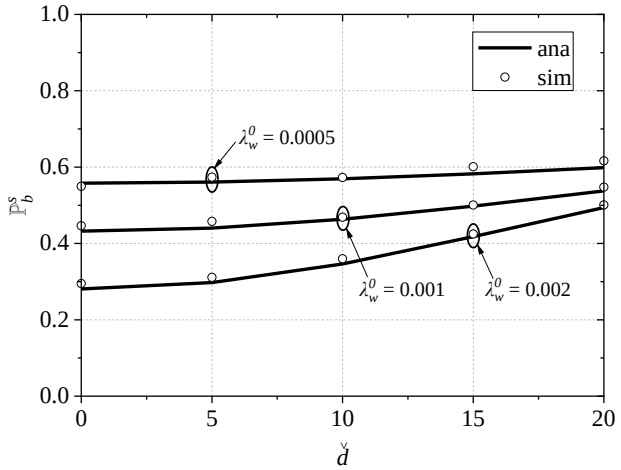

Fig. 9. $\mathbb{P}_b^s$ versus $\check{d}$ under λ_w^0 = 0.0005, 0.001, 0.002 nodes/m^2

probability $\mathbb{P}(\Psi = \psi|n)$ with $\Psi > 2$ is the same as that of $\mathbb{P}(\Psi = 2|n)$ and omitted.

- Given n, the larger L, the larger $\mathbb{P}(\Psi = 1|n)$. It is because for larger L, the tags have more possibilities to choose different backoff counters, and fewer tags choose the same minimum one. Thus, the probability of only one tag winning the contention is higher.

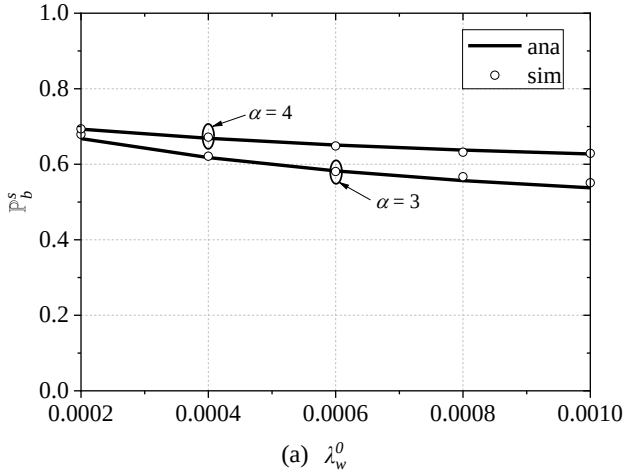

(a) λ_w^0

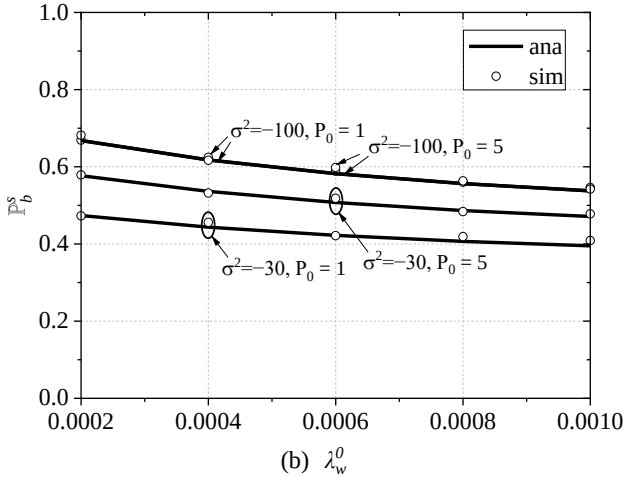

(b) λ_w^0

Fig. 10. $\mathbb{P}_b^s$ versus λ_w^0 with (a) $\alpha = 3, 4$, P_0 =1 dBm and $\sigma^2 = -100$ dBm; (b) $\alpha = 3$, $\sigma^2 = -100, -30$ dBm, and $P_0 = 1, 5$ dBm.

Fig. 8 shows the impacts of different L (i.e., $L = 4, 8, 12$) on $\bar{\Psi}$ as Λ_b varies from 1 to 30. From this figure, we can conclude:

- Given L, $\bar{\Psi}$ increases as Λ_b increases. It is because a larger Λ_b means more tags in a subcell, and thus more tags may concurrently win the contention and transmit data.
- Given Λ_b, the larger L, the smaller $\bar{\Psi}$. The reason is the same as that in Fig. 7 and omitted.

B. Successful Transmission Probability $\mathbb{P}_b^s$ of a Tag

We verify the accuracy of the lower bound of successful transmission probability $\mathbb{P}_b^s$ in (26) as the minimum distance $\check{d}$ among retained nodes, density λ_w^0 of underlying nodes and mean number Λ_b of tags in a subcell varies, under different settings of density λ_w^0, path-loss exponent α, average noise power σ^2, and reflection power P_0.

Fig. 9 shows the impacts of different λ_w^0 (i.e., λ_w^0 = 0.0005, 0.001, 0.002 nodes/m^2) on $\mathbb{P}_b^s$ as $\check{d}$ varies from 0 to 20 m. Besides, $\alpha = 3$, $L = 8$, $\Lambda_b = 5$, $\theta = 10$ dB, $P_0 = 1$ dBm, and $\sigma^2 = -100$ dBm. From this figure, we can conclude:

- Given λ_w^0, $\mathbb{P}_b^s$ increases as $\check{d}$ does. It is because that the larger $\check{d}$, the smaller density λ_w of retained nodes, and the smaller the number of retained nodes in the cell, the fewer the total number of transmitting tags in the cell, and the

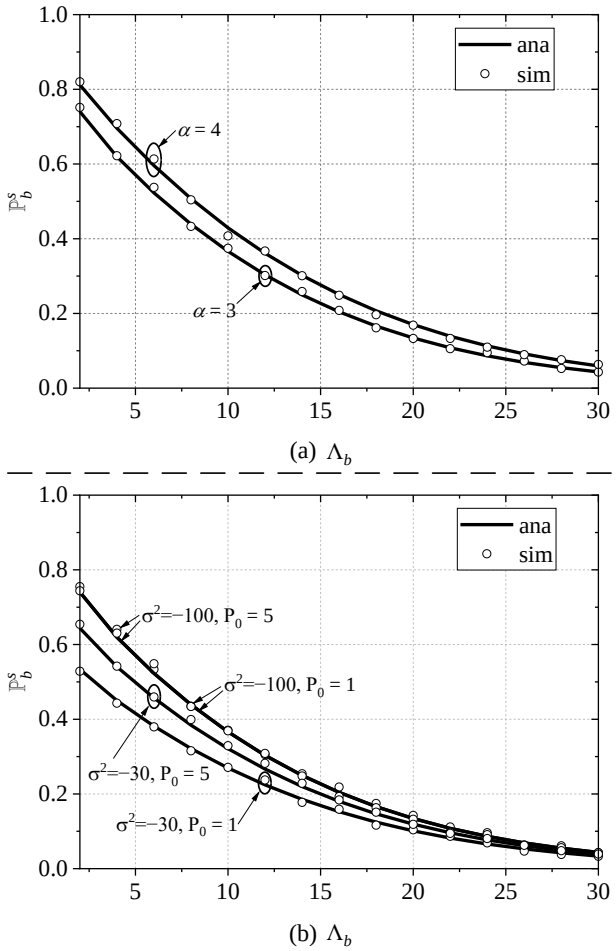

Fig. 11. $\mathbb{P}_b^s$ versus Λ_b with (a) $\alpha = 3$, 4, $\check{d}$ = 10 m, $P_0 = 1$ dBm, and $\sigma^2 = -100$ dBm and (b) $\alpha = 3$, $\check{d}$ = 10 m, $P_0 = 1, 5$ dBm and $\sigma^2 = -100, -30$ dBm.

smaller the total interference among transmitting tags, hence the higher $\mathbb{P}_b^s$.

- Given $\check{d}$, $\mathbb{P}_b^s$ increases as λ_w^0 decreases. The reason is similar as that in above and omitted.

Figs. 10(a)-(b) show the impacts of different path-loss exponent α, reflection power P_0, and noise power σ^2 on $\mathbb{P}_b^s$ as λ_w^0 varies from 0.0002 to 0.001 nodes/m^2. Besides, $\check{d}$ = 10 m, $L = 8$, $\Lambda_b = 5$ and $\theta = 10$ dB. From these two subfigures, we can conclude:

- Given α, P_0, and σ^2, $\mathbb{P}_b^s$ decreases as λ_w^0 increases, as shown in Figs. 10(a)-(b). The reason is as follows. In this setting, as λ_w^0 increases, λ_w does, the number of interfering links increases and hence the successful transmission probability $\mathbb{P}_b^s$ decreases.
- Given λ_w^0, P_0, and σ^2, the larger α, the higher $\mathbb{P}_b^s$ as shown in Fig. 10(a). The reason is that when α is large, the power of interfering signals received at the receiver is small, which leads to a high SINR and a high $\mathbb{P}_b^s$.
- Given α, λ_w^0 and P_0, $\mathbb{P}_b^s$ increases as σ^2 decreases, while given α, λ_w^0 and σ^2, $\mathbb{P}_b^s$ increases as P_0 increases, as shown in Fig. 10 (b). The reason is that decreasing σ^2 and increasing P_0 can increase SINR and hence $\mathbb{P}_b^s$.

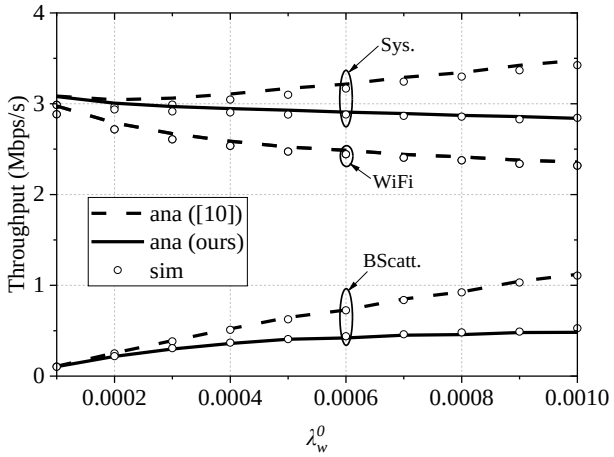

Fig. 12. Γ_s, Γ_w, and Γ_b versus λ_w^0 under $\Lambda_b = 5$.

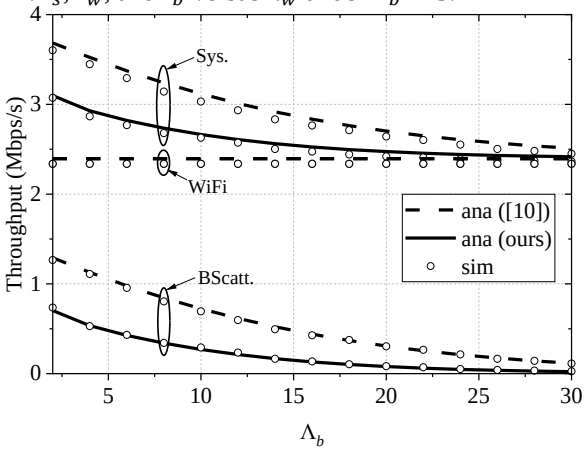

Fig. 13. Γ_s, Γ_w, and Γ_b versus Λ_b under λ_w^0 =0.0009 nodes/m^2.

- Given α and λ_w^0, when σ^2 decreases from -30 to -100 dBm, $\mathbb{P}_b^s$ increases significantly if P_0 is small (e.g., $P_0 = 1$ dBm) and increases slightly if P_0 is large (e.g., $P_0 = 5$ dBm), as shown in Fig. 10 (b). This indicates that σ^2 has a strong impact on $\mathbb{P}_b^s$ if P_0 is small.
- Given α and λ_w^0, when we improve P_0 from 1 to 5 dBm, $\mathbb{P}_b^s$ remains almost unchanged if σ^2 is very small (e.g., $\sigma^2 = -100$ dBm) and increases rapidly if σ^2 is large (e.g., $\sigma^2 = -30$ dBm), as shown in Fig. 10 (b). This implies that increasing P_0 is not an effective solution of improving $\mathbb{P}_b^s$ if σ^2 is small.

Figs. 11(a)-(b) plot the impacts of different α, P_0, and σ^2 on $\mathbb{P}_b^s$ as Λ_b varies from 2 to 30. Besides, $\lambda_w^0 = 0.0005$ nodes/m^2, d_{core} = 10, $L = 8$, $\theta = 10$ dB. From these subfigures, we have similar observations as in Figs. 10(a)-(b), which are omitted.

C. System Throughput Analysis

We now verify the accuracy of the system throughput Γ_s, WiFi throughput Γ_w, and backscatter throughput Γ_b when λ_w and Λ_b varies, under $\alpha = 3$, $L = 8$, $\check{d}$ = 10 m, $\theta = 15$ dB, $P_0 = 1$ dBm and $\sigma^2 = -100$ dBm, and compares them with those in [10]. For all figures in this subsection, labels 'Sys.', 'WiFi', 'BScatt.', '[10]', and 'ours' denote the system throughput, WiFi throughput, backscatter throughput, results in [10], and results in our work, respectively.

Fig. 12 shows the impacts of different λ_w on Γ_s, Γ_w, and Γ_b, when $\Lambda_b = 5$. From this figure, we can conclude:

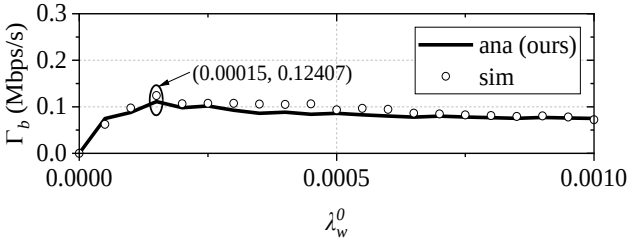

Fig. 14. Γ_b versus λ_w^0, where $\Lambda_b = 3$ tags.

- Given Λ_b, Γ_b increases as λ_w^0 increases. The reason is that as λ_w^0 increases, λ_w also increases, the number of nodes serving tags increases, thereby contributing to more concurrent tag-to-node transmissions and increasing Γ_b.
- Given Λ_b, Γ_w decreases as λ_w^0 increases. The reason is that as λ_w^0 increases, λ_w also increases, the number of nodes increases, which leads to more contention collisions, hence Γ_w decreases.
- Given Λ_b, Γ_s first decreases from 0.0001 to 0.0002 nodes/m^2 and then increases slightly as λ_w^0 increases from 0.0002 to 0.001 nodes/m^2 in [10]. The reason is as follows. Recall that $\Gamma_s = \Gamma_w + \Gamma_b$. As λ_w^0 increases from 0.0001 to 0.0002 nodes/m^2, the decrease amount of Γ_w is slightly larger than the increase amount of Γ_b. However, as λ_w^0 increases from 0.0002 to 0.001 nodes/m^2, the decrease amount of Γ_w is smaller than the increase amount of Γ_b. In contrast, Γ_s always decreases as λ_w^0 increases in our work, because the decrease amount of Γ_w is larger than the increase amount of Γ_b.

Fig. 13 plots the impacts of different Λ_b on Γ_s, Γ_w, and Γ_b as Λ_b varies, when $\lambda_w^0 = 0.0009$ nodes/m^2. From this figure, we can conclude:

- Given λ_w^0, Γ_w remains unchanged as Λ_b increases, indicating Λ_b does not impact WiFi-level communication.
- Given λ_w^0, Γ_b decreases as Λ_b increases. The reason is that as Λ_b increases, the number of interfering links increases, which decreases the successful transmission probability of tags.
- Given λ_w^0, Γ_s decreases as Λ_b increases, because Γ_s is the sum of unchanged Γ_w and decreased Γ_b.

In addition, from both Figs. 12-13, we have another two observations. First, our theoretical results closely match the corresponding simulation ones, which verifies the accuracy of our model. Second, for system and backscatter throughputs, the results in [10] are significantly different from our results, because the model in [10] assumes ideal channel conditions and does not consider the location distribution characteristics of nodes and tags, and ignores the interferences; for WiFi throughput, our results are the same as those in [10], because we mainly investigate the impact of WiFi contention on backscatter transmissions and hence adopt the same settings (including ideal channel conditions) as those in [10] to reduce the analysis complexity.

D. Parameters Optimization

In this section, we demonstrate how to exploit our theoretical model to find the optimal parameter settings. Fig. 14 shows the backscatter throughput Γ_b versus the density of WiFi nodes λ_w^0, when $\Lambda_b = 3$, $\alpha = 3$, $L = 8$, $\check{d}$ = 10 m, $\theta = 30$ dB, $P_0 = 1$ dBm, and $\sigma^2 = -100$ dBm. From this figure, we can see that Γ_b increases to a maximum value as λ_w^0 increases from 0 to 0.001 nodes/m^2 but starts decreasing when λ_w^0 continues increasing. The reason is as follows. When λ_w^0 is small, λ_w is also small, the number of concurrent tag transmissions is small, leading to a low throughput. However, when λ_w^0 is large, λ_w is also large, a great many tag transmissions will cause serious interferences, thereby lowering the throughput as well. Therefore, there exists an optimal λ_w^0 that balances concurrent tag transmissions and interferences to maximize the backscatter throughput. In this example, $\lambda_w^0 = 0.00015$ nodes/m^2 is the optimal density that maximizes Γ_b.

VIII. CONCLUSION

WiFi backscatter exploits ubiquitous WiFi signals as excitation signals to convey data and hence offers wide application prospects in many fields. However, the inherent limitations of backscatter systems, such as short transmission ranges and low throughput, have motivated the development of NWB. NWB can effectively extend the communication range of backscatter tags with forwarding assistants of WiFi nodes and greatly improve the backscatter throughput by enabling concurrent transmissions of backscatter tags. This paper proposes a theoretical model to analyze WiFi and backscatter throughputs of NWB. Our model adopts a stochastic geometry approach to capture the WiFi nodes' repulsive characteristics and backscatter tags' clustering characteristics. Besides, it accounts for the randomness and dependency of WiFi and backscatter contentions, as well as the feature of concurrent transmissions of backscatter tags. Extensive simulation results verify the accuracy of our model. This study can provide significant insights for selecting optimal parameter settings to ensure the high performance of NWB networks.

ACKNOWLEDGMENT

This work is funded in part by the Science and Technology Development Fund, Macau SAR (File No. 0093/2022/A2 and 0076/2022/A2).

REFERENCES

[1] B. Kellogg, A. Parks, S. Gollakota, J. R. Smith, and D. Wetherall, "Wi-Fi backscatter: Internet connectivity for RF-powered devices," in *Proceedings of the 2014 ACM Conference on SIGCOMM*, 2014, pp. 607–618.

[2] D. Bharadia, K. R. Joshi, M. Kotaru, and S. Katti, "Backfi: High throughput wifi backscatter," *ACM SIGCOMM Computer Communication Review*, vol. 45, no. 4, pp. 283–296, 2015.

[3] X. Yang *et al.*, "A survey on smart agriculture: Development modes, technologies, and security and privacy challenges," *IEEE/CAA Journal of Automatica Sinica*, vol. 8, no. 2, pp. 273–302, 2021.

[4] G. Franze, G. Fortino, X. Cao, G. M. L. Sarne, and Z. Song, "Resilient control in large-scale networked cyber-physical systems: Guest editorial," *IEEE/CAA Journal of Automatica Sinica*, vol. 7, no. 5, pp. 1201–1203, 2020.

[5] Q. Peng *et al.*, "Reliability-aware and deadline-constrained mobile service composition over opportunistic networks," *IEEE Transactions on Automation Science and Engineering*, vol. 18, no. 3, pp. 1012–1025, 2020.

[6] Z. Ma, L. Feng, and F. Xu, "Design and analysis of a distributed and demand-based backscatter MAC protocol for internet of things networks," *IEEE Internet of Things Journal*, vol. 6, no. 1, pp. 1246–1256, 2018.

[7] P. Zhang, D. Bharadia, K. Joshi, and S. Katti, "Hitchhike: Practical backscatter using commodity wifi," in *Proceedings of the 14th ACM Conference on Embedded Network Sensor Systems CD-ROM*, 2016, pp. 259–271.

[8] T. Adame, A. Bel, B. Bellalta, J. Barcelo, and M. Oliver, "IEEE 802.11 ah: the WiFi approach for M2M communications," *IEEE Wireless Communications*, vol. 21, no. 6, pp. 144–152, 2014.

[9] E. Khorov, A. Lyakhov, A. Krotov, and A. Guschin, "A survey on IEEE 802.11 ah: An enabling networking technology for smart cities," *Computer communications*, vol. 58, pp. 53–69, 2015.

[10] Z. Wang, L. Feng, S. Yao, K. Xie, and Y. Chen, "Low-Cost and Long-Range Node-Assisted WiFi Backscatter Communication for 5G-Enabled IoT Networks," *Wireless Communications and Mobile Computing*, vol. 2021, 2021.

[11] H. S. Dhillon, R. K. Ganti, F. Baccelli, and J. G. Andrews, "Modeling and analysis of K-tier downlink heterogeneous cellular networks," *IEEE Journal on Selected Areas in Communications*, vol. 30, no. 3, pp. 550–560, 2012, doi: 10.1109/JSAC.2012.120405.

[12] S. D. Okegbile, B. T. Maharaj, and A. S. Alfa, "Stochastic geometry approach towards interference management and control in cognitive radio network: A survey," *Computer Communications*, vol. 166, pp. 174–195, 2021.

[13] M. Haenggi, *Stochastic geometry for wireless networks*. Cambridge University Press, 2012.

[14] A.-K. Ajami and H. Artail, "Analyzing the Impact of the Coexistence With IEEE 802.11ax Wi-Fi on the Performance of DSRC Using Stochastic Geometry Modeling," *IEEE Transactions on Communications*, vol. 67, no. 9, pp. 6343–6359, Sep. 2019, doi: 10.1109/TCOMM.2019.2923411.

[15] H. Hu, Y. Gao, J. Zhang, X. Chu, and J. Zhang, "On the Performance and Fairness of LTE-U and WiFi Networks Sharing Multiple Unlicensed Channels," in *2019 IEEE 30th Annual International Symposium on Personal, Indoor and Mobile Radio Communications (PIMRC)*, Sep. 2019, pp. 1–6. doi: 10.1109/PIMRC.2019.8904396.

[16] Q. Wang, Y. Zhou, H.-N. Dai, G. Zhang, and W. Zhang, "Performance on Cluster Backscatter Communication Networks with Coupled Interferences," *IEEE Internet of Things Journal*, vol. 9, no. 20, pp. 20282–20294, Oct. 2022, doi: 10.1109/JIOT.2022.3174002.

[17] K. Han and K. Huang, "Wirelessly Powered Backscatter Communication Networks: Modeling, Coverage, and Capacity," *IEEE Transactions on Wireless Communications*, vol. 16, no. 4, pp. 2548–2561, Apr. 2017, doi: 10.1109/TWC.2017.2665629.

[18] B. Kellogg, V. Talla, J. R. Smith, and S. Gollakot, "PASSIVE WI-FI: Bringing Low Power to Wi-Fi Transmissions," *GetMobile: Mobile Comp. and Comm.*, vol. 20, no. 3, pp. 38–41, Jan. 2017, doi: 10.1145/3036699.3036711.

[19] X. Cao, Z. Song, B. Yang, M. ElMossallamy, L. Qian, and Z. Han, "A Distributed MAC Using Wi-Fi to Assist Sporadic Backscatter Communications," in *IEEE INFOCOM 2019-IEEE Conference on Computer Communications Workshops (INFOCOM WKSHPS)*, IEEE, 2019, pp. 780–785.

[20] Y. Wang, Q. Zhao, S. Yao, L. Feng, and H. Liang, "Performance Modeling of Tags-to-WiFi Transmissions for Contention-based WiFi Backscatter Networks," in *2022 IEEE International Conference on Networking, Sensing and Control (ICNSC)*, Dec. 2022, pp. 1–6. doi: 10.1109/ICNSC55942.2022.10004070.

[21] X. Zhang and M. Haenggi, "The Performance of Successive Interference Cancellation in Random Wireless Networks," *IEEE Transactions on Information Theory*, vol. 60, no. 10, pp. 6368–6388, Oct. 2014, doi: 10.1109/TIT.2014.2341248.

[22] S. Sen, N. Santhapuri, R. R. Choudhury, and S. Nelakuditi, "Successive Interference Cancellation: Carving Out MAC Layer Opportunities," *IEEE Transactions on Mobile Computing*, vol. 12, no. 2, pp. 346–357, Feb. 2013, doi: 10.1109/TMC.2012.17.

[23] G. Ghatak, S. R. Khosravirad, and A. D. Domenico, "Stochastic Geometry Framework for Ultrareliable Cooperative Communications With Random Blockages," *IEEE Internet of Things Journal*, vol. 9, no. 7, pp. 5150–5161, Apr. 2022, doi: 10.1109/JIOT.2021.3108955.

[24] H. ElSawy, E. Hossain, and S. Camorlinga, "Characterizing random CSMA wireless networks: A stochastic geometry approach," in *2012 IEEE International Conference on Communications (ICC)*, Jun. 2012, pp. 5000–5004. doi: 10.1109/ICC.2012.6363772.

[25] S. D. Okegbile, B. T. Maharaj, and A. S. Alfa, "Interference Characterization in Underlay Cognitive Networks With Intra-Network and Inter-Network Dependence," *IEEE Trans. on Mobile Comput.*, vol. 20, no. 10, pp. 2977–2991, Oct. 2021, doi: 10.1109/TMC.2020.2993408.

[26] J. Park and I. Guvenc, "Interference Analysis for UAV Radar Networks With Guard Zones Based on Stochastic Geometry," *IEEE Transactions on Aerospace and Electronic Systems*, pp. 1–31, 2023, doi: 10.1109/TAES.2023.3236308.

[27] C. Lee and M. Haenggi, "Interference and Outage in Poisson Cognitive Networks," *IEEE Transactions on Wireless Communications*, vol. 11, no. 4, pp. 1392–1401, Apr. 2012, doi: 10.1109/TWC.2012.021512.110131.

[28] M. Haenggi, "Mean Interference in Hard-Core Wireless Networks," *IEEE Communications Letters*, vol. 15, no. 8, pp. 792–794, Aug. 2011, doi: 10.1109/LCOMM.2011.061611.110960.

[29] R. K. Ganti and M. Haenggi, "Interference and Outage in Clustered Wireless *Ad Hoc* Networks," *IEEE Trans. Inform. Theory*, vol. 55, no. 9, pp. 4067–4086, Sep. 2009, doi: 10.1109/TIT.2009.2025543.

[30] X. Peng, C. Ren, G. Chen, and L. Qiu, "Analysis of Clustered Multi-Antenna Small Cells With Intra-Cluster Interference Cancellation," *IEEE Transactions on Vehicular Technology*, vol. 68, no. 11, pp. 11343–11347, Nov. 2019, doi: 10.1109/TVT.2019.2936038.

[31] J. Tang, G. Chen, J. P. Coon, and D. E. Simmons, "Distance distributions for Matérn cluster processes with application to network performance analysis," in *2017 IEEE International Conference on Communications (ICC)*, May 2017, pp. 1–6. doi: 10.1109/ICC.2017.7997055.

[32] J. Tang, G. Chen, and J. P. Coon, "Joint Coverage Enhancement by Power Allocation in Poisson Clustered Out-of-Band D2D Networks," *IEEE Transactions on Vehicular Technology*, vol. 67, no. 12, pp. 11537–11548, Dec. 2018, doi: 10.1109/TVT.2018.2871065.

[33] X. Cao, Z. Song, B. Yang, M. A. Elmossallamy, L. Qian, and Z. Han, "A Distributed Ambient Backscatter MAC Protocol for Internet-of-Things Networks," *IEEE Internet of Things Journal*, vol. 7, no. 2, pp. 1488–1501, Feb. 2020, doi: 10.1109/JIOT.2019.2955909.

[34] V. Liu, A. Parks, V. Talla, S. Gollakota, D. Wetherall, and J. R. Smith, "Ambient Backscatter: Wireless Communication Out of Thin Air," *ACM SIGCOMM Computer Communication Review*, vol. 43, no. 4, pp. 39–50, Oct. 2013.

[35] M. Chu, A. Liu, J. Chen, V. K. N. Lau, and S. Cui, "A Stochastic Geometry Analysis for Energy-Harvesting-Based Device-to-Device Communication," *IEEE Internet Things J.*, vol. 9, no. 2, pp. 1591–1607, Jan. 2022, doi: 10.1109/JIOT.2021.3091723.

[36] X. Zhang and J. G. Andrews, "Downlink Cellular Network Analysis With Multi-Slope Path Loss Models," *IEEE Transactions on Communications*, vol. 63, no. 5, pp. 1881–1894, 2015.

[37] Y. Liu, H.-N. Dai, M. Imran, and N. Nasser, "Ground-to-UAV Communication Network: Stochastic Geometry-based Performance Analysis," in *ICC 2021 - IEEE International Conference on Communications*, Montreal, QC, Canada: IEEE, Jun. 2021, pp. 1–6. doi: 10.1109/ICC42927.2021.9500746.

[38] N. Deng, W. Zhou, and M. Haenggi, "Heterogeneous Cellular Network Models With Dependence," *IEEE J. Select. Areas Commun.*, vol. 33, no. 10, pp. 2167–2181, Oct. 2015, doi: 10.1109/JSAC.2015.2435471.

[39] G. Bianchi, "Performance analysis of the IEEE 802. 11 distributed coordination function," *IEEE Journal on selected areas in communications*, vol. 18, no. 3, pp. 535–547, 2000.

[40] A. Kumar, E. Altman, D. Miorandi, and M. Goyal, "New Insights From a Fixed-Point Analysis of Single Cell IEEE 802.11 WLANs," *IEEE/ACM Transactions on Networking*, vol. 15, no. 3, pp. 588–601, Jun. 2007, doi: 10.1109/TNET.2007.893091.

[41] Q. Zhao, D. H. Tsang, and T. Sakurai, "A simple and approximate model for nonsaturated IEEE 802.11 DCF," *IEEE Transactions on Mobile Computing*, vol. 8, no. 11, pp. 1539–1553, 2009.

[42] Q. Zhao, D. H. Tsang, and T. Sakurai, "Modeling nonsaturated IEEE 802.11 DCF networks utilizing an arbitrary buffer size," *IEEE Transactions on Mobile Computing*, vol. 10, no. 9, pp. 1248–1263, 2010.

[43] B. Błaszczyszyn, M. Haenggi, P. Keeler, and S. Mukherjee, *Stochastic Geometry Analysis of Cellular Networks*, 1st ed. Cambridge University Press, 2018. doi: 10.1017/9781316677339.

Yulei Wang received his B.S. degree from University of Science and Technology Beijing, Beijing, China, in 2015, and M.S. degree from Macau University of Science and Technology (MUST), Macau, China, in 2019. He is currently pursuing the Ph.D. degree in MUST. His current research interests include wireless networks and stochastic geometry.

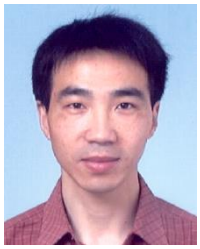

Qinglin Zhao received his Ph.D. degree from the Institute of Computing Technology, the Chinese Academy of Sciences, Beijing, China, in 2005. From May 2005 to August 2009, he worked as a postdoctoral researcher at the Chinese University of Hong Kong and the Hong Kong University of Science and Technology. Since September 2009, he has been with the School of Computer Science and Engineering at Macau University of Science and Technology and now he is a professor. He serves as an associate editor of IEEE Transactions on Mobile Computing and IET Communications. His research interests include blockchain and decentralization computing, machine learning and its applications, Internet of Things, wireless communications and networking, cloud/fog computing, software-defined wireless networking.

Shumin Yao received his Ph.D. and M.S. degrees from Macau University of Science and Technology, Macau, China, in 2022 and 2018, respectively, and his B.S. degree from Beijing Institute of Technology, Zhuhai, China, in 2016. He is currently a Postdoctoral researcher in Peng Cheng Laboratory, Shenzhen, China. His interests include wireless LAN and Internet of Things.

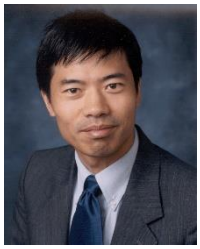

MengChu Zhou (Fellow, IEEE) received his Ph. D. degree from Rensselaer Polytechnic Institute, Troy, NY in 1990 and then joined New Jersey Institute of Technology where he is now a Distinguished Professor. His interests are in Petri nets, automation, Internet of Things, and big data. He has over 1100 publications including 14 books, 750+ journal papers (600+ in IEEE transactions), 31 patents and 32 book-chapters. He is Fellow of IFAC, AAAS, CAA and NAI.

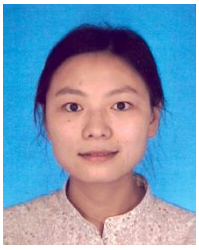

Li Feng received her M.S. degree in operation research from the Department of Mathematics, University of Hong Kong, Hong Kong, in 2007, and her Ph.D. degree in electronic information technology from the School of Computer Science and Engineering (SCSE), Macau University of Science and Technology (MUST), Macao, China, in 2013. She is currently an Associate Professor in SCSE, MUST. Her current research interests include Internet of Things, wireless and mobile networks, power saving, software defined networking, and performance analysis.

Peiyun Zhang (M'16–SM'17) received her Ph.D. in computer science from the School of Computer Science and Technology at the Nanjing University of Science and Technology, Nanjing, China in 2008. She is currently a professor at the Engineering Research Center of Digital Forensics of Ministry of Education, and the School of Computer Science, Nanjing University of Information Science & Technology. Her interests include blockchains, and cloud/ trust computing. She has published over 70 papers in these fields.